Real-Time Detection of Open-Phase Conditions in the Onsite Power System of a Nuclear Power Plant Using a Two-stage CNN-Based Framework

Gipyo Kweon, Junsang Cha, Seokjun Kang, and Gilsoo Jang
Department of Electrical Engineering
Korea University
Seoul, Korea
dogi2009@korea.ac.kr, wnstkd916@korea.ac.kr, seokjun0107@korea.ac.kr, and gjang@korea.ac.kr

***Abstract*—Open-Phase Condition (OPC) is a critical abnormal event in the onsite power system of a Nuclear Power Plant (NPP) that is challenging to detect via conventional protection relays due to transformer voltage regeneration. This paper proposes a real-time, convolutional neural network (CNN)-based two-stage diagnostic framework for OPC detection. The first-stage performs Power Quality Disturbance (PQD) detection, serving a dual purpose by simultaneously providing real-time PQD surveillance and acting as a precursor trigger for potential OPC events. The second-stage, an event classification model employing a signal processing technique, is activated selectively by a checkpoint mechanism. This hierarchical processing structure significantly reduces the computational burden while maintaining real-time operability, making the proposed framework highly suitable for practical deployment in the onsite power systems of NPPs.**

***Index Terms*—Convolutional neural network, discrete wavelet transform, fault detection, open-phase condition, and power quality.**

I. Introduction

Open-phase conditions (OPCs) typically occur due to the loss of one or two primary phases feeding the transformer caused by various physical or operational faults in nuclear power plants (NPPs) [1]. Following the Byron NPP open-phase event in 2012, it was revealed that OPCs can persist undetected for extended periods due to the complex electromagnetic coupling and voltage regeneration characteristics within transformer [2]. In particular, the magnetic flux in the core of the healthy phases can partially regenerate voltage on the open phase [3]. The extent of voltage regeneration varies significantly depending on several factors: system earthing arrangements, properties of cables and overhead lines, location of the open phase, transformer core construction type (3-limbs, 5-limbs, or Shell), winding connection (Y-Y or Δ-Y), and load level (heavy or light) [4]. Under certain operating conditions, only slight deviations in voltages and currents may be observable even during an OPC. As a result, OPCs can remain undetected for extended periods, leading to asymmetric loading, transformer winding overheating, and magnetic core saturation, thereby increasing the risk of equipment failure and cascading system disruptions. In [5], OPC detection schemes have been proposed, however these approaches generally rely on upgrading or incorporating additional complex functions in relay logic.

Concurrently, as modern nuclear power plants increasingly integrate non-linear loads and DC equipment, onsite power systems are exposed to harmonics and other disturbances. This trend has heightened the operational demand for real-time monitoring of Power Quality Disturbances (PQDs), defined as deviations in voltage, current, and frequency from standard ratings [6]. While recent studies have successfully employed convolutional neural network (CNN) based approaches to

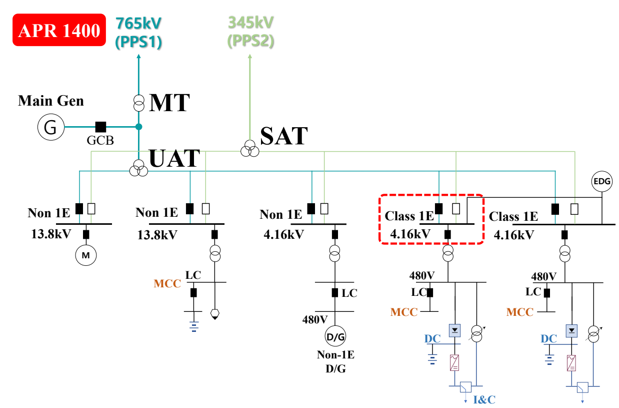

Figure 1. Schematic diagram of the APR1400 onsite power system.

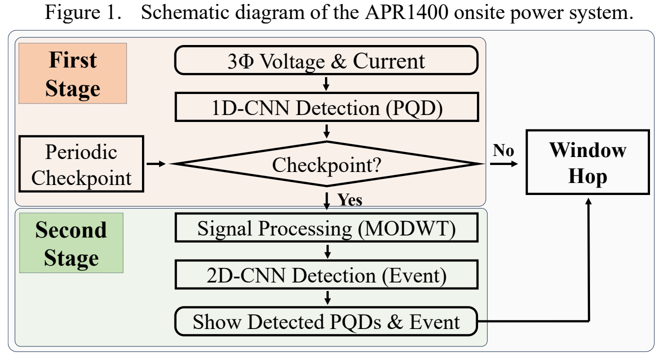

Figure 2. Flowchart of the proposed two-stage detection framework.

This work was supported by the National Research Foundation of Korea(NRF) grant funded by the Korea government(MSIT) (No. RS-2023-00218377).

979-8-3315-8138-1

interpret these raw waveform signatures [7], [8], this study advances these methods by proposing an integrated diagnostic framework. This framework serves a dual purpose: fulfilling the operator's requirement for Power Quality (PQ) surveillance while simultaneously leveraging this comprehensive PQ information to effectively detect OPCs.

This paper presents a data-driven diagnostic framework using 6-channel data (3-phase voltages and currents) from a single load bus (4.16 kV Class 1E bus). As illustrated in Fig. 1, simulations utilized a high-fidelity PSCAD/EMTDC model of the APR1400 Saeul NPP in Korea [9]. Authentic design parameters were incorporated to compensate for the limited operational data. Specifically, the Main Transformer (MT) employs a Y-Δ configuration, and the Standby Auxiliary Transformer (SAT) is modeled as a shell-type Y-Y-Y transformer with buried delta windings, both of which are notably vulnerable to voltage regeneration [4].

As depicted in Fig. 2, the diagnostic process adopts a hierarchical two-stage architecture employing a sliding window technique for real-time monitoring. In the first stage, checkpoints are triggered via dual-mechanism: a 1-D CNN scans raw waveforms to detect PQDs associated with distinctive OPCs and generate checkpoints, while periodic checkpoints are generated every 5 cycles to ensure the capture of stealthy OPCs. Upon checkpoint generation, the second stage initiates a detailed analysis using the Maximal Overlap Discrete Wavelet Transform (MODWT) to extract time-frequency features for event classification by a 2-D CNN. This selective activation strategy significantly reduces the computational burden by engaging signal processing only when necessary.

The main contributions are summarized as follows:

- Dual-Purpose PQD Monitoring: Simultaneously delivers real-time PQ surveillance for operators and leverages PQD signals as precursor triggers for potential OPCs, maximizing operational utility.
- Threshold-Free Hierarchical Detection: Integrates two specialized CNN models to eliminate manual threshold settings, ensuring robust performance even against grid noise.
- Computationally Efficient Architecture: Optimizes the accuracy-efficiency trade-off via a parallel checkpoint mechanism that activates detailed analysis only on demand, minimizing computational burden.

II. FIRST-STAGE: POWER QUALITY DETECTION

A. *Power Quality Disturbance Data Generation*

The first-stage is designed to detect PQDs within a 5-cycle time window (83.3ms) and provide an activation signal to the second stage. A total of 12 classes of PQ are considered, excluding flicker-related classes reported in previous studies such as [7] and [8]. This exclusion is justified by the absence of large, rapidly fluctuating loads in the onsite power systems of NPPs.

TABLE I. MATHEMATICAL FORMULATIONS OF POWER QUALITY DISTURBANCES

Label	PQ Class	Mathematical Formulations	Parameters	
C1	Normal	$x(t) = sin\omega_0 t$	$\omega_0 = 2\pi f_0, f_0 = 60\ (Hz)$	
C2	Sag	$x(t) = (1 + \alpha w(t)) \cdot sin\omega_0 t$	$-0.9 \le \alpha \le -0.1$	$w(t)$: raised-cosine window (smoothing window)
C3	Swell		$0.1 \le \alpha \le 0.8$	
C4	Interruption		$-1.0 \le \alpha \le -0.9$	
C5	Harmonics	$x(t) = sin\omega_0 t + w(t)[a_3 sin(3\omega_0 t + \varphi_3) + a_5 sin(5\omega_0 t + \varphi_5) + a_7 sin(7\omega_0 t + \varphi_7)]$	$0.03 \le a_3 \le 0.10$, $0.02 \le a_5 \le 0.08$, $0.01 \le a_7 \le 0.06$	
C6	Sag & Harmonics	$x(t) = (1 + \alpha w(t)) \cdot sin\omega_0 t + w(t)[a_3 sin(3\omega_0 t + \varphi_3) + a_5 sin(5\omega_0 t + \varphi_5) + a_7 sin(7\omega_0 t + \varphi_7)]$	$-0.9 \le \alpha \le -0.1$, $0.03 \le a_3 \le 0.10$, $0.02 \le a_5 \le 0.08$, $0.01 \le a_7 \le 0.06$	
C7	Swell & Harmonics		$0.1 \le \alpha \le 0.8$, $0.03 \le a_3 \le 0.10$, $0.02 \le a_5 \le 0.08$, $0.01 \le a_7 \le 0.06$	
C8	Interruption & Harmonics	$x(t) = (1 + \alpha w(t)) \cdot sin\omega_0 t + \frac{1}{2} w(t)[a_3 sin(3\omega_0 t + \varphi_3) + a_5 sin(5\omega_0 t + \varphi_5) + a_7 sin(7\omega_0 t + \varphi_7)]$	$-1.0 \le \alpha \le -0.9$, $0.03 \le a_3 \le 0.10$, $0.02 \le a_5 \le 0.08$, $0.01 \le a_7 \le 0.06$	
C9	Oscillatory Transient	$x(t) = sin\omega_0 t + \alpha e^{-\frac{t-t_1}{\tau}} sin(2\pi f_T(t - t_1)) \cdot [u(t - t_1) - u(t - t_2)]$	$0.05 \le \alpha \le 4$, $300 \le f_T \le 5000$ (Hz) $0.3 \le t_2 - t_1 \le 50$ (ms), $\tau = \frac{t_2 - t_1}{r}$, $r \in [2,5]$	
C10	Impulsive Transient	$x(t) = sin\omega_0 t + \sum_{i=1}^{n_p} u_i(t)$, $u_i(t) = A_i \frac{t - t_{0,i}}{t_r}[u(t - t_{0,i}) - u(t - (t_{0,i} + t_r))] + A_i e^{-\frac{t-(t_{0,i}+t_r)}{t_i}} u(t - (t_{0,i} + t_r))$	$1 \le n_p \le 2$, $0.1 \le A_i \le 0.5$ $0 \le t_{0,i} \le 0.0833$ (s), $t_r = 0.1$ (ms), $1 \le t_i \le 5$ (ms)	
C11	Periodic Notch	$x(t) = sin\omega_0 t - \alpha \cdot sign(sin\omega_0 t) \cdot r(t)$, $r(t) = \begin{cases} 1, & t_1 \le t_{in} < t_1 + \Delta \\ 0, & Otherwise \end{cases}$, $t_{in} = t \cdot mod \frac{T}{2}$	$0.1 \le \alpha \le 0.4$, $0.01T \le \Delta \le 0.05T$ $0 \le t_1 \le \frac{T}{2} - \Delta$	
C12	Spike	$x(t) = sin\omega_0 t + \alpha \cdot sign(sin\omega_0 t) \cdot r(t)$, $r(t) = \begin{cases} 1, & t_1 \le t_{in} < t_1 + \Delta \\ 0, & Otherwise \end{cases}$, $t_{in} = t \cdot mod \frac{T}{2}$	$0.1 \le \alpha \le 0.4$, $0.01T \le \Delta \le 0.05T$ $0 \le t_1 \le \frac{T}{2} - \Delta$	

979-8-3315-8138-1

Flicker is defined as "the subjective impression of fluctuating luminance caused by voltage fluctuations" [10], which makes it difficult to express mathematically. All remaining PQD definitions were refined in Table I, based on earlier studies to match precisely with the IEEE Std 1159-2019 classification.

To enable robust real-time detection using a sliding window, the model must identify both the onset and termination of PQDs, rather than solely detecting continuous disturbances (C2–C8). Accordingly, the dataset includes stochastically generated waveforms representing three scenarios: full-span PQDs persisting across the entire 5-cycle window, boundary-straddling PQDs positioned near the window edges, and short-duration disturbances that emerge and dissipate within the window. For impulsive transients (C10), multiple impulse occurrences were synthesized by introducing an adjustable parameter. As summarized in TABLE III, 100,000 waveforms were generated for each class. To emulate realistic measurement and communication environments, random noise with a Signal-to-Noise Ratio (SNR) ranging from 20 to 60 dB was injected into the dataset.

B. *Model Architecture of Power Quality Detection Stage*

The first-stage model architecture adopts the deep 1D-CNN proposed in [7], which demonstrated high classification accuracy. The same architecture was applied to the newly formulated PQ waveforms to evaluate whether the deep 1D-CNN could maintain robust performance when trained on more detailed PQD patterns. The detailed hyperparameters and performance metrics are summarized in Table II and detailed dataset information is presented in Table III. The quantitative performance metrics, including accuracy, F1-score, false positive rate, and false negative rate are summarized in TABLE V.

C. *Sliding Window and Parallel Checkpoint Mechanism*

Sliding window method begins once 833 samples (5-cycle) of data have been accumulated. The window then moves with a hop size of 1/12 cycle (1.4ms) to perform PQD detection on each channel, as illustrated in Fig. 3. The 1D-CNN model performs reliably when the window primarily contains steady-state channel data. However, during transitional periods in which a PQD is beginning or ending, the classification confidence of model may momentarily decrease because the sliding window does not yet contain sufficient representative samples, leading to temporarily unstable predictions. Once enough samples enter the window, the model converges to the correct class label.

The same sliding window method is applied to all 6 channels to detect PQDs within the same time frame. If any of 6 channels detects a PQD in its window, a PQD-driven checkpoint is generated, which triggers the second-stage model for event classification. In addition, period-driven checkpoints are generated every 5 cycles to prevent missing stealthy OPCs that may not be categorized as distinct PQDs.

TABLE II. ARCHITECTURE OF THE PQD-DETECTION CNN

Layer Block	Layer Type	Configuration (Filters, Kernel/Stride)	Activation
Input	Raw Signal	1 Channel	-
Unit 1	Conv1D x 2	32 filters, 3x1/1	ReLU
	Max Pooling	3x1/3	-
	Batchnorm	-	-
Unit 2	Conv2D	64 filters, 3x1/1	ReLU
	Max Pooling	3x1/3	-
	Batchnorm	-	-
Unit 3	Conv2D	128 filters, 3x1/1	ReLU
	Adap. Pooling	Global	-
Classifier	Fully Connected	256	ReLU
	Fully Connected	128	ReLU
	Output Layer	12	Softmax

TABLE III. SUMMARY OF DATASET

Stage	Waveform Conditions	No. of Total Dataset	No. of Test Dataset
I	12 PQ Classes	1,200,000 (100,000 per class)	60,000
II	7 Event Classes · Full Load (100%) · Light Load (10%) · Full Load (0%)	210,000 (10,000 per class)	21,000

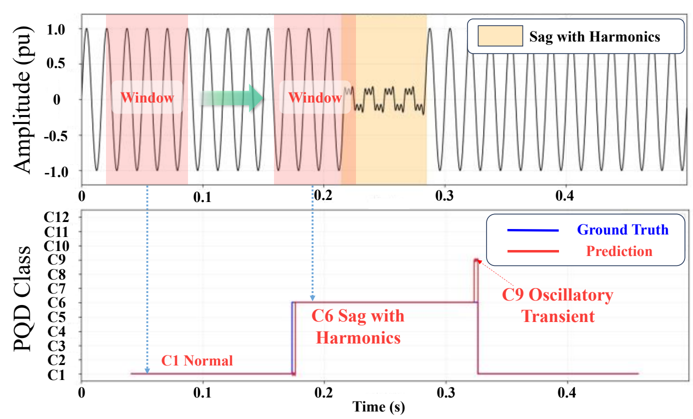

Figure 3. Real-time sliding window validation of PQDs on a single channel.

III. SECOND-STAGE: EVENT DETECTION

A. *Event Data Acquisition*

Using a precisely developed PSCAD/EMTDC model of the Saeul NPP Units, 6-channel data consisting of 3-phase voltages and 3-phase currents were extracted from the 4.16 kV Class 1E bus. The dataset defines seven distinct event classes: a normal state, three single-phase OPCs (phases A, B, C), and three double-phase OPCs (phases AB, BC, CA). Given that OPC characteristics are sensitive to transformer loading, simulations were

979-8-3315-8138-1

conducted across three scenarios: Full Load (100%), Light Load (10%), and No Load (0%). To ensure a comprehensive dataset, 10,000 samples were generated for each class by randomizing event-trigger times and extracting multiple 5-cycle waveform segments on specific event, as detailed in Table III. Finally, to emulate realistic operating environments, random noise with 20-60 dB SNR was injected into the extracted waveforms.

B. Signal Processing with Discrete Wavelet Transform

The Discrete Wavelet Transform (DWT) enables multi-resolution analysis suitable for identifying small signal deviations [11]. In this study, MODWT was adopted over the standard DWT. Unlike the standard DWT, MODWT avoids downsampling, preserving time alignment and accommodating arbitrary sample sizes [12]. Although MODWT lacks orthogonality, this trade-off is acceptable as it ensures consistent input dimensions suitable for the 2D-CNN model.

Using the Daubechies-4 (db4) mother wavelet, a 4-level MODWT is applied to each single-channel waveform. This decomposition level is selected as an optimal trade-off between frequency resolution and boundary distortion. Lower levels provide insufficient frequency separation, whereas higher levels increase edge-effect distortion, necessitating excessive data truncation. The 4-level decomposition achieves adequate separation while limiting boundary removal, resulting in 729 valid samples. Fig. 4 illustrates the MODWT-processed coefficients of an A-phase voltage during an OPC. Note that while the coefficients in the figure were normalized for visualization, the actual training dataset retains the original magnitudes to preserve relative signal characteristics across frequency bands and channels.

C. Model Architecture of Event Detection Stage

The second-stage model architecture was designed as a 2D-CNN to simultaneously capture information from both the time and frequency domains. The specific architectural details, including layer configurations and kernel dimensions, are summarized in TABLE IV. As shown, the model features a streamlined architecture designed to maximize classification performance while maintaining structural simplicity. To capture the complex relationships among the 6-channel data during OPCs, all channels were used together as a single multichannel input to the model. Shared convolutional kernels were applied across the channels so that the learned weights could represent inter-channel dependencies, which are essential for distinguishing different OPC classes. The quantitative performance metrics of the second-stage model are presented in TABLE V. After training, the 2D-CNN model achieved an accuracy of 99.85% on time-aligned 6-channel window snapshots, demonstrating reliable discriminative performance for OPC event classification.

IV. VALIDATION

While the discriminative performance of the individual CNN models was evaluated using a snapshot-based validation dataset in TABLE V, the actual real-time detection capability of the integrated framework is demonstrated through the time-domain analysis shown in Fig. 6 and Fig. 7. To assess this real-time applicability, 1-second 6-channel waveforms were generated using PSCAD/EMTDC, encompassing all OPC classes, where each scenario contained either a Normal condition or a randomly triggered OPC.

Fig. 6 illustrates the framework response to an A-phase OPC under a full-load condition. In the pre-fault region, periodic checkpoints are correctly classified as normal. Upon fault initiation, the first-stage detects PQDs, and as the window captures sufficient post-transition samples, the second-stage output converges to the correct OPC class. Similarly, Fig. 7 demonstrates a C-phase OPC under a no-load condition. Despite the subtle signal deviations inherent to this scenario, the framework successfully detects the fault.

Considering that an OPC often evolves into a ground fault when a detached conductor contacts the earth, the framework was validated against scenarios where high-resistance ground faults (10 kΩ, 100 kΩ, 1,000 kΩ) occur simultaneously with OPCs. This rigorous validation confirms reliability of the framework in realistic scenarios.

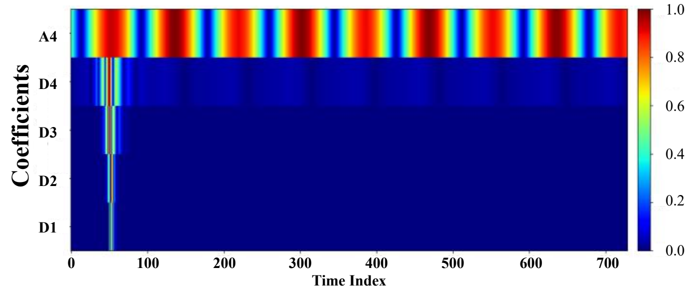

Figure 4. MODWT coefficients of A-phase voltage under an A-phase OPC.

TABLE IV. ARCHITECTURE OF THE EVENT-DETECTION CNN

Layer Block	Layer Type	Configuration (Filters, Kernel/Stride)	Activation
Input	Signal Processed Data	6 Channel	-
Unit 1	Conv2D	64 filters, 3x3/1	ReLU
	Max Pooling	1x2/2	-
Unit 2	Conv2D	128 filters, 3x3/1	ReLU
	Max Pooling	1x2/2	-
Unit 3	Conv2D	256 filters, 3x3/1	ReLU
	Adap. Pooling	Global	-
Classifier	Fully Connected	128 (Dropout 0.4)	ReLU
	Output Layer	7	Softmax

TABLE V. PERFORMANCE METRICS OF CNN MODELS

Stage	Accuracy (%)	F1-Score	False Positive Rate (%)	False Negative Rate (%)
I	99.49	98.98	0.38	0.52
II	99.85	99.91	0.13	0.16

V. Discussion

- Single-Point Measurement: Relying on multi-point measurements imposes a significant computational burden due to the increased channel count and introduces complex time-synchronization issues. To avoid these overheads, this study utilizes single-point measurements from a Class 1E bus, prioritizing field applicability.
- Scope of Study: Simulations were confined to OPCs during steady-state operations to establish a clear baseline for feature extraction. Verification against simultaneous disturbances or power swings is needed for future research.

VI. Conclusion

This paper presents a real-time two-stage framework for detecting OPCs in the APR1400 onsite power system. The proposed framework establishes a dual-purpose architecture that simultaneously delivers real-time PQ surveillance and utilizes these signals as precursor triggers for OPC detection. This integrated design allows for practical implementation using only 6-channel waveform measurements from a single point, thereby optimizing computational efficiency. Extensive validation using PSCAD/EMTDC demonstrates that the architecture robustly identifies OPCs across diverse operating scenarios, thereby verifying the feasibility of applying AI-based monitoring systems to a critical power system.

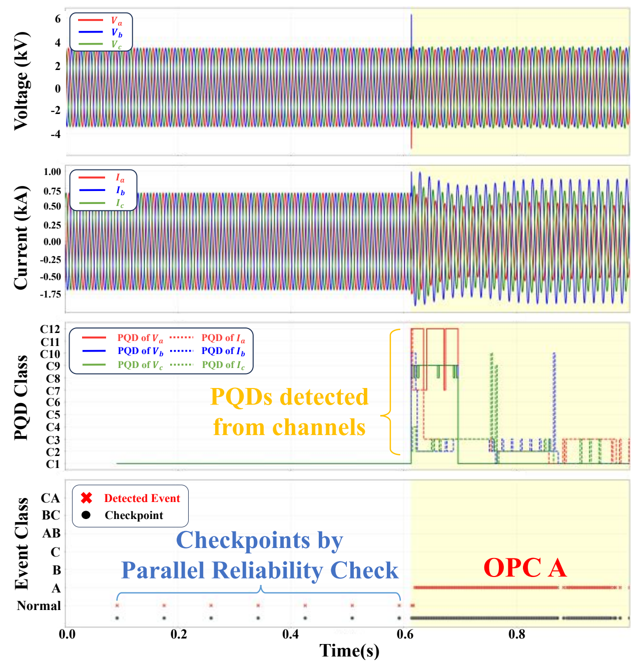

Figure 6. Real-time validation scenario: A-phase OPC under Full-Load.

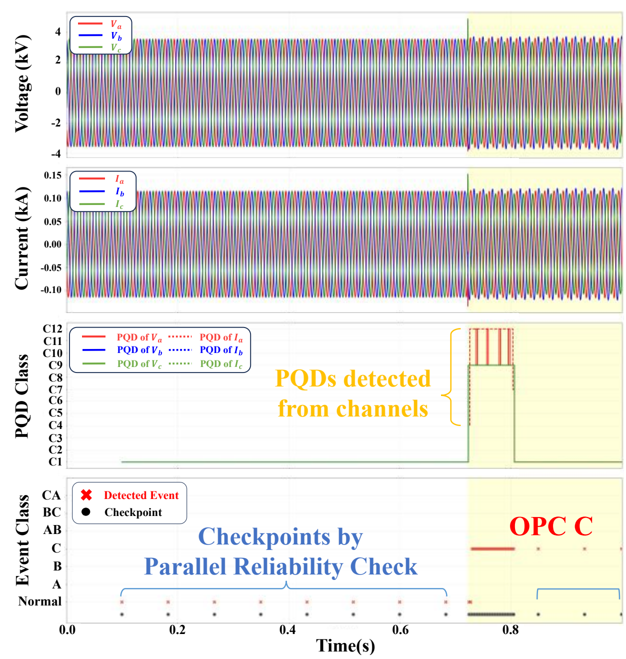

Figure 7. Real-time validation scenario: C-phase OPC under No-Load.

References

[1] Abed, Nagy Y., Frank Ashrafi, and Kyle Chang. "Simulation and detection of open phase for generating station auxiliary three phase transformers." *2014 IEEE PES General Meeting Conference & Exposition*. IEEE, 2014.

[2] Johnson, W. "Nuclear maintenance application center: Development and analysis of an open-phase detection scheme for various configurations of auxiliary transformers." EPRI, Palo Alto, CA, USA, Tech. Rep. 3002000764, 2013.

[3] IAEA. "Impact of Open Phase Conditions on Electrical Power Systems of Nuclear Power Plants." IAEA, 2017.

[4] IEEE PSRC Working Group K11, "Methods for Analyzing and Detecting an Open Phase Condition of a Power Circuit to a Nuclear Plant Station Service or Startup Transformer," IEEE Power System Relaying and Control Committee, Piscataway, NJ, Tech. Rep. WG K11, 2018.

[5] Cox, A. Dwayne, and H. Chaluvadi. "Open-phase detection for station auxiliary transformers." Proc. Annual Western Protective Relay Conference, 2018.

[6] Mahela, Om Prakash, Abdul Gafoor Shaik, and Neeraj Gupta. "A critical review of detection and classification of power quality events." *Elsevier Renewable and Sustainable Energy Reviews*, Vol. 41, pp. 495-505, 2015.

[7] Shouxiang Wang, Haiwen Chen, "A novel deep learning method for the classification of power quality disturbances using deep convolutional neural network," *Elsevier Applied Energy*, vol. 235, pp. 1126-1140, 2019.

[8] N. M. Rodrigues, F. M. Janeiro and P. M. Ramos, "Deep Learning for Power Quality Event Detection and Classification Based on Measured Grid Data," in *IEEE Transactions on Instrumentation and Measurement*, vol. 72, pp. 1-11, 2023.

[9] Korea Electric Power Corp. (KEPCO) and Korea Hydro & Nuclear Power Co., Ltd (KHNP), "Onsite AC power system analysis," Tech. Rep. APR1400-E-E-NR-14001-NP, Rev. 3, Jan. 2018.

[10] *IEEE Recommended Practice for Monitoring Electric Power Quality*, IEEE Std. 1159-2019, June. 2019.

[11] Suhail Khokhar, Abdullah Asuhaimi Mohd Zin, Aslam Pervez Memon, Ahmad Safawi Mokhtar, "A new optimal feature selection algorithm for classification of power quality disturbances using discrete wavelet transform and probabilistic neural network", *Elsevier Measurement*, Vol. 95, pp. 246-259, 2017.

[12] Dghais, Amel Abdoullah Ahmed, and Mohd Tahir Ismail. "A comparative study between discrete wavelet transform and maximal overlap discrete wavelet transform for testing stationarity". *Int J. Math. Comput. Sei.* Eng 7, pp. 1184-1188, 2013.